Nonlinear ponderomotive scattering of relativistic electrons by an intense laser field at focus

F. V. Hartemann, S. N. Fochs, G. P. Le Sage, and N. C. Luhmann, Jr.
Department of Applied Science, University of California, Davis, California 95616

J. G. Woodworth, M. D. Perry, and Y. J. Chen
Lawrence Livermore National Laboratory, Livermore, California 94550

A. K. Kerman
Center for Theoretical Physics, Laboratory for Nuclear Science and Department of Physics, Massachusetts Institute of Technology, Cambridge, Massachusetts 02139

(Received 24 October 1994)

The relativistic dynamics of electrons subjected to the electromagnetic field of an intense, ultrashort laser pulse in vacuum is studied theoretically. The effects of both finite pulse duration and beam focusing are taken into account. It is found that when the quiver amplitude of the electrons driven by the laser field exceeds the focal spot radius of a Gaussian beam, the restoring force acting on the charge decays exponentially, and the electrons are scattered away from the focus. This physical process, known as ponderomotive scattering, effectively terminates the interaction within a laser wavelength, and the electrons can escape with very high energy, as the normalized laser field is of the order of or greater than unity. The relation between the scattering angle and the escape energy is derived analytically from the conservation of canonical momentum and energy in the photon field. For a linearly polarized laser field, the interaction produces two jets of high energy electrons. The theory is supplemented by detailed two-dimensional computer simulations.

PACS number(s): 52.40.Nk, 42.50.Vk, 52.75.Di, 42.65.−k

I. INTRODUCTION

The recent advent of extremely high intensity, ultrafast lasers using fiber compression [1], Kerr-lens mode locking [2], and, more recently, chirped pulse amplification [3,4] has renewed the interest in laser acceleration for future linear colliders. A number of acceleration schemes have been proposed that use different geometries to efficiently mediate the electron-photon interaction. Recent experimental results have validated these schemes by demonstrating high gradient laser-electron scattering in a plasma beat-wave configuration [5] or in a plasma wake field [6]. These proposals also include the concept of free-wave acceleration known as nonlinear inverse bremsstrahlung, where the electrons interact with the laser field and an externally applied field in a vacuum [7–9]. The applied field can either be reversed periodically, as in a tapered inverse free-electron laser [10], or remain uniform.

The focus of this paper is the theoretical study of the interaction of an extremely intense, pulsed laser field (normalized field of the order of or greater than unity) with a single electron, in vacuum, in the vicinity of the focus. In this electrodynamic system, two very different regimes are possible. At lower laser intensity, in the linear regime, the transverse quiver amplitude of the electron is small, and the effects of the transverse spatial gradients in the vicinity of focus are essentially negligible. In this case, the net kinetic energy gain for the electrons scattered by the ponderomotive potential is very small, as discussed extensively in the literature [11–16]. In the case of a standing wave, the electron is Bragg scattered, as first predicted by Kapitza and Dirac [17]. This first-order linear effect has been observed by Bucksbaum, Schumacher, and Bashkansky [18]. In the high-intensity limit, or nonlinear regime, the situation is fundamentally different: the quiver amplitude imparted by the laser wave to the electron becomes comparable to the beam waist at focus, and the electron can be scattered away with a high escape energy, since the laser-electron interaction is effectively terminated within a wavelength λ. This phenomenon has been simulated in computer calculations [19], but was not identified as nonlinear ponderomotive scattering. As will be shown in Sec. IV, the power threshold P^* for this process can be estimated by equating the relativistic quiver amplitude to the beam waist w_0, with the result that

$$P^* \approx \frac{\pi^5}{\gamma_0^2}\left[\frac{\varepsilon_0 m_0^2 c^5}{e^2}\right]\left[\frac{w_0}{\lambda}\right]^4 ,$$

where γ_0 is the normalized injection energy of the scattered electron. This threshold numerically translates into

$$P^* \approx \frac{0.21}{\gamma_0^2}\left[\frac{w_0}{\lambda}\right]^4 TW .$$

This physical process will be referred to as high-intensity ponderomotive wave (HPW) scattering in the remainder of this paper. An experimental observation of this effect, at low electron energy (< 80 keV), has been reported [20].

The problem is first studied analytically in the simple case of a linearly polarized plane wave with a temporal envelope, and the maximum electron energy is shown to scale linearly with the laser intensity and with the injection energy. The theoretical framework for this electrodynamic system is constructed within the framework of classical electrodynamics and special relativity. This framework is appropriate because the average number of photons scattered by an electron is very high, and the photon field can be essentially treated as a classical, continuous electromagnetic field. The theory is then supplemented by detailed computer simulations, taking into account the transverse excursion of the accelerated electron in the plane of polarization, the temporal structure of the ultrashort laser pulse, and the effects of diffraction. The comparison of the analytical theory with the computer simulations enables us to benchmark the computer code.

In the two-dimensional analysis, we consider a relativistic electron traveling along the propagation axis of the wave. The electron motion is studied in the plane of polarization. The electron is overtaken by the laser pulse close to the focus, and its energy is modulated as it experiences the various phases of the electromagnetic field. In the focusing region, the laser field amplitude increases rapidly because of both spatial (focusing) and temporal (slippage towards the center of the pulse) effects. As a result, the quiver amplitude increases exponentially, but the particle is still confined around the propagation axis because the restoring force increases with the driving force. In close proximity to the focus, however, this situation can become unstable if the quiver amplitude exceeds the focal spot radius. In this case, as the electron quivers through the spatial gradient of the Gaussian laser field, the restoring force decays exponentially, and the particle can be scattered away from the focus, with a high energy. This scattering mechanism is studied in detail with a two-dimensional computer code. It is found that there is a simple correlation between the scattering angle and the escape energy of the electron. This correlation is then expressed analytically, and explained by using the invariance of the canonical momentum in the photon field.

This paper is organized as follows. In Sec. II, we present an analytical derivation of the relativistic dynamics of an electron submitted to the electromagnetic field of a plane wave laser pulse. We first briefly review the main results in the case of an infinitely long pulse (no temporal envelope variations). We than analyze the case of a finite-duration pulse. These results are then used to benchmark the two-dimensional computer simulations, which are presented in detail in Sec. III. In Sec. IV, we use the computer simulations to study the scattering mechanism in a number of possible experimental configurations. Finally, conclusions are drawn in Sec. V.

II. PLANE WAVE ANALYSIS

In this section, we review the dynamics of a relativistic electron submitted to an intense, finite-duration, plane wave, linearly polarized laser pulse. We first start with a brief overview of the main results obtained for a plane wave with no temporal envelope.

A. Review of a continuous plane wave

The electron normalized velocity, normalized energy, and momentum are defined as

$$\boldsymbol{\beta}=\frac{\mathbf{v}}{c},\quad \gamma=\frac{1}{\sqrt{1-\boldsymbol{\beta}^2}},\quad \mathbf{p}=\gamma m_0 c\boldsymbol{\beta}\ .$$

Neglecting radiation damping [21], the energy-momentum transfer equations are

$$d_t\mathbf{p}=-e(\mathbf{E}+\mathbf{v}\times\mathbf{B})\ , \tag{1}$$

$$d_t\gamma=\frac{-e}{m_0c^2}\mathbf{v}\cdot\mathbf{E}\ . \tag{2}$$

We now consider a linearly polarized plane wave propagating *in vacuo:*

$$\mathbf{E}=\hat{\mathbf{x}}E_0(\phi)\sin\phi\ , \tag{3}$$

$$\mathbf{B}=\hat{\mathbf{y}}\frac{E_0(\phi)}{c}\sin\phi\ , \tag{4}$$

where we have defined the electron phase in terms of the laser frequency ω,

$$\phi(t)=\omega\left[t-\frac{z(t)}{c}\right]\ . \tag{5}$$

With this, the energy-momentum transfer equations are expressed as

$$d_t(\gamma\beta_x)=\frac{-eE_0}{m_0c}(1-\beta_z)\sin\phi\ , \tag{6}$$

$$d_t(\gamma\beta_y)=0\ , \tag{7}$$

$$d_t(\gamma\beta_z)=\frac{-eE_0}{m_0c}\beta_x\sin\phi\ , \tag{8}$$

$$d_t\gamma=\frac{-eE_0}{m_0c}\beta_x\sin\phi\ . \tag{9}$$

From Eq. (7) we have $\beta_y=\text{const}=0$. Subtracting Eq. (8) from Eq. (9), we find the invariant

$$d_t[\gamma(1-\beta_z)]=0\ , \tag{10}$$

$$\gamma(1-\beta_z)=\text{const}=\gamma_0(1-\beta_0)\ , \tag{11}$$

where γ_0 and β_0 are the normalized injection energy and velocity, respectively. In addition, we have by definition

$$\frac{1}{\gamma^2}=1-\beta_x^2-\beta_z^2\ . \tag{12}$$

It is the straightforward to show that

$$\gamma(\phi)=\gamma_0\left[1+[\gamma\beta_x(\phi)]^2\left[\frac{1+\beta_0}{2}\right]\right]\ . \tag{13}$$

This equation is valid as long as we are considering plane waves.

At this point, it is important to notice that

$$d_t\phi=\omega(1-\beta_z)\ ; \tag{14}$$

therefore Eq. (6) can be integrated with respect to ϕ,

which is now treated as an independent variable. We find, with the appropriate initial conditions,

$$\gamma\beta_x(\phi)=\alpha(\cos\phi-1) , \tag{15}$$

where we have introduced the normalized laser field strength

$$\alpha=\frac{eE_0}{\omega m_0 c}=\frac{eE_0\lambda}{2\pi m_0 c^2} . \tag{16}$$

Here, λ is the laser wavelength.

We now proceed to derive γ, β_x, and β_z from Eqs. (11), (13), and (15). After some straightforward algebra, we find

$$\gamma(\phi)=\gamma_0\left[1+\alpha^2(\cos\phi-1)^2\left[\frac{1+\beta_0}{2}\right]\right] , \tag{17}$$

$$\beta_x(\phi)=\frac{2\alpha(\cos\phi-1)}{\gamma_0[2+\alpha^2(1+\beta_0)(\cos\phi-1)^2]} , \tag{18}$$

$$\beta_z(\phi)=1-\frac{2(1-\beta_0)}{2+\alpha^2(1+\beta_0)(\cos\phi-1)^2} . \tag{19}$$

It is easily verified that at $t=0$, the following initial conditions are satisfied:

$$z(t=0)=0, \quad \phi(t=0)=0, \quad \gamma(t=0)=\gamma_0 ,$$

$$\beta_x(t=0)=0 \quad \beta_z(t=0)=\beta_0 .$$

The maximum energy of the electron in the laser field is attained at $\phi=(2n+1)\pi$ and has the value

$$\gamma^*=\gamma_0[1+2\alpha^2(1+\beta_0)] . \tag{20}$$

Using the well-known relation between the laser field and intensity I,

$$E_0=\sqrt{2I/\varepsilon_0 c} , \tag{21}$$

the maximum normalized electron energy in the laser field is then given by

$$\gamma^*=\gamma_0\left[1+I\lambda^2\frac{e^2}{\pi^2\varepsilon_0 m_0^2 c^5}(1+\beta_0)\right] . \tag{22}$$

For relativistic electrons, the maximum energy scales linearly with the injection energy, reflecting the fact that at high energy the electron remains synchronous with the wave for a longer time as it is injected with a velocity close to the speed of light. At high laser intensities, the maximum electron energy also scales linearly with I.

The temporal evolution of the nonlinear phase is obtained by using Eq. (14) and replacing β_z by its expression given in Eq. (19). We obtain a nonlinear first-order differential equation

$$d_t\phi=\frac{2\omega(1-\beta_0)}{2+\alpha^2(1+\beta_0)(\cos\phi-1)^2} . \tag{23}$$

This equation can be solved analytically by the separation of variables; the result is given in Eq. (32). We now proceed to derive a number of important characteristics of the electron trajectory by using ϕ as the independent variable. The transverse excursion of the electron in the laser field can be derived as follows. We have

$$\frac{dx}{d\phi}=\frac{dx}{dt}\frac{dt}{d\phi}=\frac{c\beta_x}{\omega(1-\beta_z)} . \tag{24}$$

Multiplying both the numerator and denominator of this ratio by γ, we obtain

$$\frac{dx}{d\phi}=\frac{c\alpha(\cos\phi-1)}{\omega\gamma_0(1-\beta_0)} . \tag{25}$$

Equation (25) can easily be integrated analytically, which results in

$$x(\phi)=\frac{c\alpha}{\omega\gamma_0(1-\beta_0)}\int_0^{\phi}(\cos u-1)du=\frac{c\alpha(\sin\phi-\phi)}{\omega\gamma_0(1-\beta_0)} . \tag{26}$$

The evolution of the axial electron position as a function of the phase can also be derived in a similar way. We have

$$\frac{dz}{d\phi}=\frac{dz}{dt}\frac{dt}{d\phi}=\frac{c\gamma\beta_z}{\omega\gamma_0(1-\beta_0)} . \tag{27}$$

Replacing γ and β_z by their values, Eq. (27) reduces to

$$\frac{dz}{d\phi}=\frac{c}{2\omega(1-\beta_0)}[2\beta_0+\alpha^2(1+\beta_0)(\cos\phi-1)^2] . \tag{28}$$

We now use the identity

$$1-\cos\phi=2\sin^2\frac{\phi}{2} , \tag{29}$$

which yields the following differential equation for z:

$$\frac{dz}{d\phi}=\frac{c}{\omega(1-\beta_0)}\left[\beta_0+2\alpha^2(1+\beta_0)\sin^4\frac{\phi}{2}\right] . \tag{30}$$

Equation (30) is easily integrated [22], with the result that

$$z(\phi)=\frac{c}{\omega(1-\beta_0)}\left\{\phi[\beta_0+\tfrac{3}{4}\alpha^2(1+\beta_0)]+\alpha^2(1+\beta_0)\left[\frac{\sin 2\phi}{8}-\sin\phi\right]\right\} . \tag{31}$$

By using the definition of the nonlinear phase [Eq. (5)] and replacing $z(t)$ by the solution given in Eq. (31), we can replace the nonlinear differential equation governing the evolution of the phase [Eq. (23)] by a transcendental equation in ϕ,

$$\phi=\omega t-\frac{1}{1-\beta_0}\left\{\phi[\beta_0+\tfrac{3}{4}\alpha^2(1+\beta_0]+\alpha^2(1+\beta_0)\left[\frac{\sin 2\phi}{8}-\sin\phi\right]\right\} . \tag{32}$$

The evolution of the electron energy, velocity, and position as a function of phase is illustrated in Figs. 1–3 for $\alpha=3$ and $\gamma_0=10$.

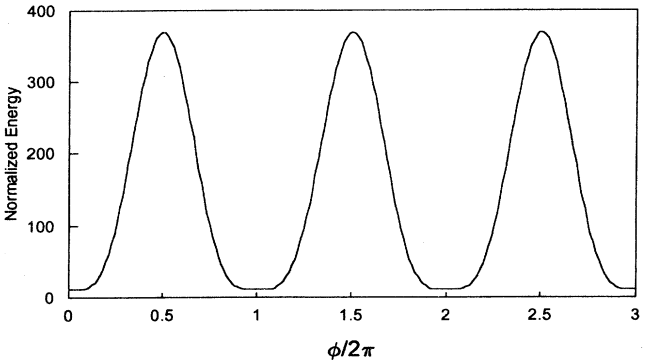

FIG. 1. One-dimensional evolution of the electron normalized energy as a function of phase, for $\alpha=3$, $\gamma_0=10$ and no temporal envelope.

B. Finite-duration pulses

We now consider a laser pulse with finite duration. The electric and magnetic field associated with the laser are

$$\mathbf{E}=\hat{\mathbf{x}}E_0 g(\phi)\sin\phi \ , \tag{33}$$

$$\mathbf{B}=\hat{\mathbf{y}}\frac{E_0}{c}g(\phi)\sin\phi \ , \tag{34}$$

where the function $g(\phi)$ represents the temporal envelope of the laser pulse. The relativistic energy-momentum transfer equations can be expressed as

$$d_t(\gamma\beta_x)=-\alpha\omega(1-\beta_z)g(\phi)\sin\phi \ , \tag{35}$$

$$d_t(\gamma\beta_z)=-\alpha\omega\beta_x g(\phi)\sin\phi \ , \tag{36}$$

$$d_t\gamma=-\alpha\omega\beta_x g(\phi)\sin\phi \ . \tag{37}$$

Subtracting Eq. (36) from Eq. (37), we recover the invariant given in Eq. (11), namely

$$\gamma(1-\beta_z)=\gamma_0(1-\beta_0) \ . \tag{38}$$

By using Eqs. (12) and (38), we can show that

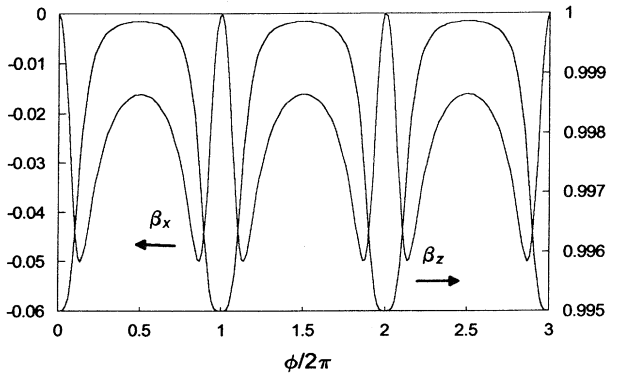

FIG. 2. One-dimensional evolution of the electron normalized velocity as a function of phase, for $\alpha=3$, $\gamma_0=10$ and no temporal envelope.

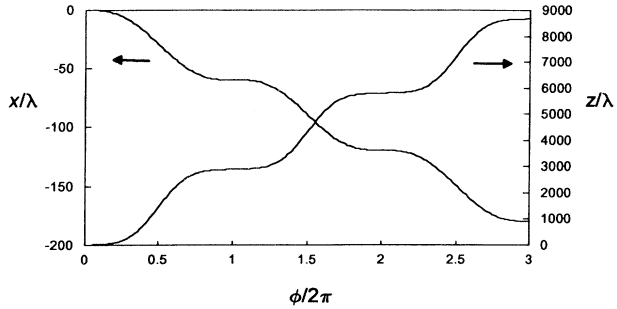

FIG. 3. One-dimensional evolution of the electron normalized transverse and axial position as a function of phase, for $\alpha=3$, $\gamma_0=10$ and no temporal envelope.

$$\gamma(\phi)=\gamma_0\left\{1+\alpha^2\left[\int_0^{\phi}g(u)\sin(u)du\right]^2\left[\frac{1+\beta_0}{2}\right]\right\} . \tag{39}$$

This equation holds as long as plane waves are considered.

For the sake of simplicity, we now assume a cosine envelope of duration $\Delta\tau$,

$$g(\phi)=E_0\cos^2\left[\frac{\pi}{2}\left[\frac{\phi}{\omega\Delta\tau}-1\right]\right] . \tag{40}$$

Equation (39) can now be integrated analytically, with the result that

$$[\gamma\beta_x](\phi)=a(\phi)\sin\phi+b(\phi)\cos\phi+q \ , \tag{41}$$

where we have defined

$$a(\phi)=p\kappa\sin\left[\pi\left[\frac{\phi}{\Delta\phi}-1\right]\right] , \tag{42}$$

$$b(\phi)=p\cos\left[\pi\left[\frac{\phi}{\Delta\phi}-1\right]\right]+\frac{\alpha}{2} , \tag{43}$$

$$q=\kappa^2 p \ . \tag{44}$$

Here, we have introduced $\Delta\phi=\omega\Delta\tau$ and the quantities

$$\kappa=\frac{\pi}{\Delta\phi}, \quad p=\frac{\alpha}{2}\frac{1}{1-\kappa^2} \ .$$

The maximum energy attained by the electron in the laser wave is approximately given by

$$\gamma^*=\gamma_0\left[1+\alpha^2\left[\frac{1+\beta_0}{2}\right]\right] , \tag{45}$$

where we have neglected the terms in κ. This equation is very similar to the one derived in the case of a continuous wave, but the effective normalized wave amplitude is reduced by a factor of 2.

The transverse excursion of the electron as a function of the phase can be derived as follows. The quiver amplitude is governed by the differential equation

$$\frac{dx}{d\phi}=\frac{dx}{dt}\frac{dt}{d\phi}=\frac{c[\gamma\beta_x(\phi)]}{\omega\gamma_0(1-\beta_0)} \ . \tag{46}$$

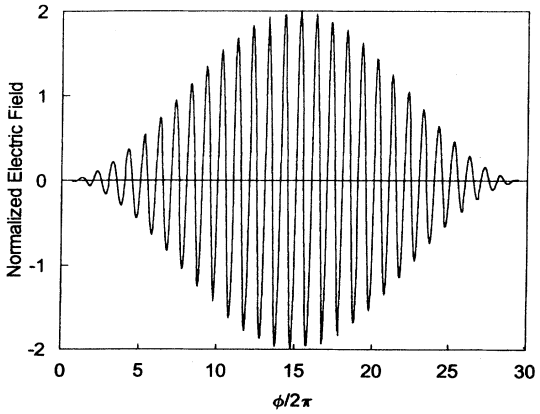

FIG. 4. Normalized electric field of the laser wave as a function of phase for $I=0.055$ TW/μm^2, $\lambda=1$ μm, and $\Delta\tau=50$ fs.

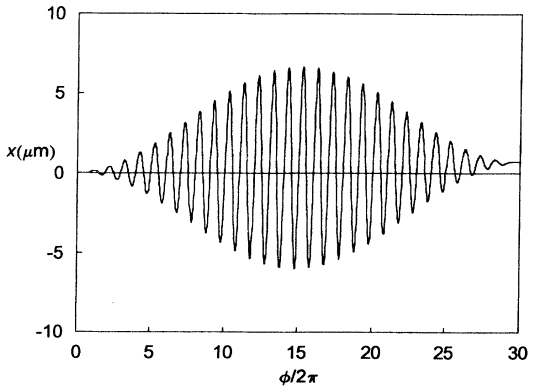

FIG. 6. Transverse electron trajectory as a function of phase, from 1D theory, for a finite-duration laser pulse. The laser parameters are the same as in Fig. 4, and $\gamma_0=10$.

With the appropriate boundary condition $[x(\phi=0)=0]$, we find that

$$x(\phi)=\gamma_0(1+\beta_0)\frac{\lambda}{2\pi}\int_0^{\phi}[a(u)\sin u+b(u)\cos u+q]du\ , \tag{47}$$

which can be integrated analytically. The result can be written in the form

$$x(\phi)=\gamma_0(1+\beta_0)\frac{\lambda}{2\pi}[A(\phi)+B(\phi)+q\phi]\ , \tag{48}$$

where we have defined

$$A(\phi)=\frac{p\kappa}{2(1-\kappa^2)}[(\kappa-1)\sin(\phi+\kappa\phi-\kappa\Delta\phi) -(\kappa+1)\sin(-\phi+\kappa\phi-\kappa\Delta\phi) -2\sin(\kappa\Delta\phi)]\ , \tag{49}$$

$$B(\phi)=\frac{p}{2(\kappa^2-1)}[(\kappa-1)\sin(\phi+\kappa\phi-\kappa\Delta\phi) +(\kappa+1)\sin(-\phi+\kappa\phi-\kappa\Delta\phi) +\kappa\sin(\kappa\Delta\phi)]+\frac{\alpha}{2}\sin\phi\ . \tag{50}$$

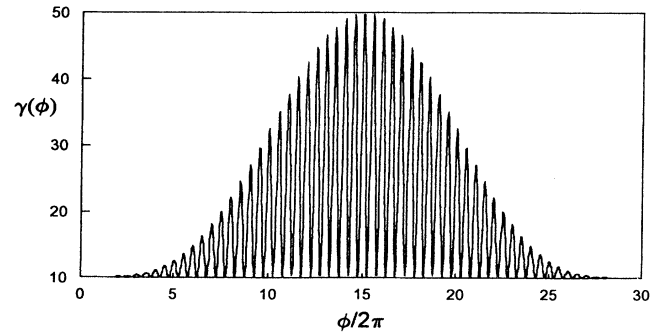

FIG. 5. Normalized electron energy as a function of phase, from 1D theory, for a finite-duration laser pulse. The laser parameters are the same as in Fig. 4, and $\gamma_0=10$.

The maximum relativistic quiver amplitude can then be closely approximated by

$$x^*\approx\alpha\gamma_0(1+\beta_0)\frac{\lambda}{2\pi}\ . \tag{51}$$

To illustrate the derivations presented above, we have evaluated the dynamical parameters of a relativistic electron (normalized injection energy $\gamma_0=10$) as a function of its phase in the laser field for the following set of parameters. The laser wavelength is 1μm, the laser intensity is 0.55×10^{19} W/cm^2, and the pulse duration full width at half maximum (FWHM) is 50 fs. The results are shown in Figs. 4–6. In Fig. 4, the normalized electric field of the laser wave is shown as a function of phase. The normalized electron energy is shown in Fig. 5, and its quiver amplitude is presented in Fig. 6. The normalized laser field is $\alpha=2$, and the estimates for γ^* and x^* are 50 and 6.35 μm, respectively. These estimates are seen to be in excellent agreement with the analytical solutions. In addition, a small, systematic drift is observed in the transverse direction, which corresponds to the nonzero value of the parameter q [see Eq. (44)].

III. TWO-DIMENSIONAL COMPUTER CODE

In this section, we derive and discuss the main equations used in the two-dimensional computer code designed to simulate the dynamics of a relativistic electron at the focus of a short-duration, intense laser pulse. The geometry of the interaction is shown in Fig. 7. The problem is entirely two-dimensional since the laser field in the vicinity of the focus is described by the paraxial ray approximation for a linearly polarized Gaussian beam [23]

$$\mathbf{E}(x,z,t)=\hat{\mathbf{x}}\frac{E_0\exp[-x^2/w^2(z)]}{\sqrt{1+(z/z_0)^2}}g(\phi) \times\sin\left[\phi+\frac{kx^2}{2R(z)}-\arctan\left[\frac{z}{z_0}\right]\right]\ , \tag{52}$$

$$\mathbf{B}(x,z,t)=\hat{\mathbf{y}}\frac{E(x,z,t)}{c}\ . \tag{53}$$

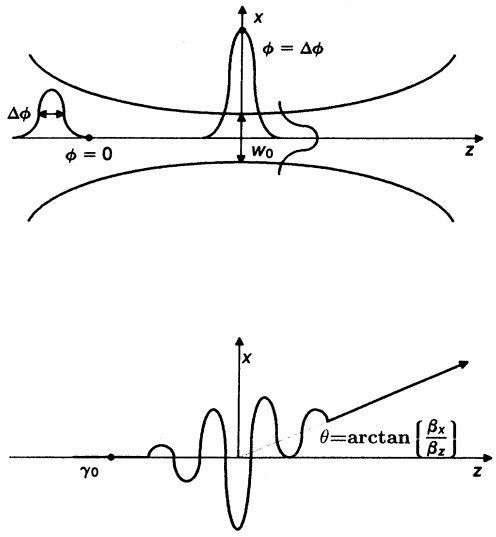

FIG. 7. Top: Schematic of the scattering process. Bottom: geometry of HPW scattering.

Here $g(\phi)$ is the temporal pulse envelope and $k=2\pi/\lambda$ is the laser wave number. We have introduced the Rayleigh range

$$z_0=\pi\frac{w_0^2}{\lambda}\ , \tag{54}$$

the beam waist

$$w(z)=w_0\left[1+\left[\frac{z}{z_0}\right]^2\right]^{1/2}\ , \tag{55}$$

and the radius of the converging and diverging spherical wave fronts

$$R(z)=z+\frac{z_0^2}{z}\ . \tag{56}$$

Here, w_0 represents the beam waist at focus ($z=0$). The electric field associated with the wave is related to the peak laser power through the relation

$$P=\pi\varepsilon_0 cE_0^2\int_0^\infty r\exp[-2(r/w_0)^2]dr=\frac{\pi}{4}\varepsilon_0 cE_0^2 w_0^2\ . \tag{57}$$

To ensure computational stability, the relativistic energy-momentum transfer equations are solved as a function of phase, which is considered as the independent variable, and normalized as follows:

$$d_\phi(\gamma\beta_x)=-\alpha G(\chi,\xi)g(\phi)\sin[\phi+\varepsilon(\chi,\xi)]\ , \tag{58}$$

$$d_\phi(\gamma\beta_z)=d_\phi(\gamma)$$
$$=-\alpha f\beta_x G(\chi,\xi)g(\phi)\sin[\phi+\varepsilon(\chi,\xi)]\ . \tag{59}$$

Here, we have introduced the following normalized variables

$$\chi(\phi)=2\pi\frac{x(\phi)}{\lambda}=kx(\phi),\quad \xi(\phi)=2\pi\frac{z(\phi)}{\lambda}=kz(\phi)\ ,$$

and the normalized functions

$$f(\phi)=\frac{1}{1-\beta_z(\phi)}=\frac{\gamma^2(1+\beta_z)}{1+(\gamma\beta_x)^2}\ , \tag{60}$$

$$\varepsilon(\chi,\xi)=\frac{1}{2}\frac{\xi\chi^2}{\xi^2+(kz_0)^2}-\arctan(\xi)\ , \tag{61}$$

$$G(\chi,\xi)=\frac{\exp\{-(\chi/kw_0)^2[1+(\xi/kz_0)^2]^{-1}\}}{\sqrt{1+(\xi/kz_0)^2}}\ . \tag{62}$$

In the above, f is a large parameter associated with the relativistic Doppler upshift, ε corresponds to the spherical wave front curvature in the vicinity of focus, and G is the Gaussian spatial transverse envelope of the beam.

In order to increase the accuracy of the code, we use a second-order Taylor expansion

$$h(\phi+\delta\phi)=h(\phi)+\delta\phi d_\phi[h(\phi)]$$
$$+\frac{\delta\phi^2}{2}d_\phi^2[h(\phi)]+O(\delta\phi^3)\ . \tag{63}$$

Here, $h(\phi)$ represents any generic function of ϕ. To obtain the second-order derivatives of $\gamma\beta_x$, $\gamma\beta_z$, and γ, we differentiate Eqs. (58) and (59) with respect to the phase. Neglecting $d_\phi\varepsilon$ and $d_\phi G$, which are slowly varying functions of the phase, we find

$$d_\phi^2(\gamma\beta_x)=-\alpha[g(\phi)\cos\phi+\sin\phi d_\phi g(\phi)]\ , \tag{64}$$

$$d_\phi^2(\gamma)=-\alpha f[\{[d_\phi(\beta_x)+f\beta_x d_\phi(\beta_z)]g(\phi)$$
$$+\beta_x d_\phi(g)\}\sin\phi+\beta_x g(\phi)\cos\phi]\ , \tag{65}$$

$$d_\phi^2(\gamma\beta_z)=d_\phi^2(\gamma)\ . \tag{66}$$

The derivative of the temporal envelope with respect to the phase is

$$d_\phi g(\phi)=-\frac{\pi}{2\Delta\phi}\sin\left[\pi\left[\frac{\phi}{\Delta\phi}-1\right]\right]\ . \tag{67}$$

The other derivatives in Eqs. (64) and (65) are given by

$$d_\phi\beta_x(\phi)=\frac{1}{\gamma}[d_\phi(\gamma\beta_x)-\beta_x d_\phi\gamma]\ , \tag{68}$$

$$d_\phi\beta_z(\phi)=\frac{1}{\gamma}[d_\phi(\gamma\beta_z)-\beta_z d_\phi\gamma]\ . \tag{69}$$

The normalized axial and transverse coordinates of the electron are governed by the following differential equations in ϕ:

$$\frac{d\chi}{d\phi}=k\frac{dx}{dt}\frac{dt}{d\phi}=f\beta_x\ , \tag{70}$$

$$\frac{d\xi}{d\phi}=k\frac{dz}{dt}\frac{dt}{d\phi}=f\beta_z\ . \tag{71}$$

The corresponding second-order derivatives are

$$d_\phi^2\chi=f[d_\phi(\beta_x)+f\beta_x d_\phi(\beta_z)]\ , \tag{72}$$

$$d_\phi^2\xi=f^2 d_\phi\beta_z\ . \tag{73}$$

The integration procedure employed in the computer code is the following. The electron initial position and velocity correspond to the initial phase $\phi=0$, when the

laser pulse starts to overtake the particle, as shown in Fig. 7. The numerical integration is performed from $\phi=0$ to $\phi=2\pi$, when the electron is no longer interacting with the wave. At each computational step, the fields are evaluated at the electron position and used to compute the first- and second-order derivatives of the dynamical quantities with respect to phase. These quantities are then updated through the second-order Taylor expansion described in Eq. (63), as well as the normalized electron coordinates. A check on the accuracy is performed by evaluating

$$\Delta(\phi+\delta\phi)=\left|2\frac{\{\gamma(\phi+\delta\phi)-[1-\beta_x^2(\phi+\delta\phi)-\beta_z^2(\phi+\delta\phi)]^{-1/2}\}}{\{\gamma(\phi+\delta\phi)+[1-\beta_x^2(\phi+\delta\phi)-\beta_z^2(\phi+\delta\phi)]^{-1/2}\}}\right| . \tag{74}$$

Typically, for $\delta\phi=2\pi\times10^{-3}$, $\Delta\leq10^{-6}$.

The code can now be benchmarked against the one-dimensional (1D) analytical theory presented in Sec. II B by choosing a very large value for the beam waist at focus. To illustrate the computer code presented above, we have evaluated the dynamical parameters of a relativistic electron (normalized injection energy $\gamma_0=10$) as a function of its phase in the laser field for the following set of parameters. The laser wavelength is 1 μm, the peak laser intensity is set at 0.55×10^{19} W/cm^2, the pulse duration (FWHM) is 50 fs, and the beam waist at focus is 1 mm. The normalized electron energy is shown in Fig. 8, and the transverse quiver motion is presented in Fig. 9. The simulation results are in excellent agreement with the analytical solutions presented in Figs. 5 and 6, and demonstrate the validity of the code in the 1D limit.

IV. LASER-ELECTRON PONDEROMOTIVE SCATTERING

In this two-dimensional analysis, we consider a relativistic electron traveling along the propagation axis of the wave. The spatial envelope of the laser field in the focus region is modeled by a Gaussian beam, and the temporal envelope is a raised cosine. The laser wave is linearly polarized.

In this electrodynamic system, two very different regimes are possible. At low laser intensity, the transverse quiver amplitude of the electron is small, and the effects of the transverse spatial gradients in the vicinity of focus are essentially negligible. In this case, there is no net kinetic-energy gain for the electrons, and the results closely resemble those found in the one-dimensional case, as the transverse motion of the electron is confined in a region of space which is much smaller than the laser beam waist. In the high power limit, however, the situation is fundamentally different: the quiver amplitude imparted by the laser wave to the electron becomes comparable to the beam waist at focus, and the electron can be scattered away with a high escape energy, as the laser-electron interaction is effectively terminated within a wavelength.

The power threshold P^* for HPW scattering can be estimated by equating the relativistic quiver amplitude [see Eq. (51)] to the beam waist w_0, with the result that

$$P^*\approx\frac{\pi^5}{\gamma_0^2}\left[\frac{\varepsilon_0 m_0^2c^5}{e^2}\right]\left[\frac{w_0}{\lambda}\right]^4 , \tag{75}$$

where γ_0 is the normalized injection energy of the scattered electron. This threshold numerically translates into

$$P^*\approx\frac{0.21}{\gamma_0^2}\left[\frac{W_0}{\lambda}\right]^4 TW .$$

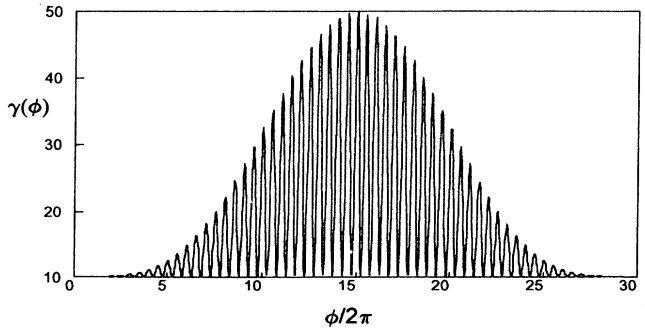

FIG. 8. Normalized electron energy as a function of phase, from 2D simulations. The laser parameters are $\alpha=2$, $\lambda=1$ μm, $\Delta\tau=50$ fs, and $w_0=1$ mm. The electron is injected at focus with a normalized energy $\gamma_0=10$.

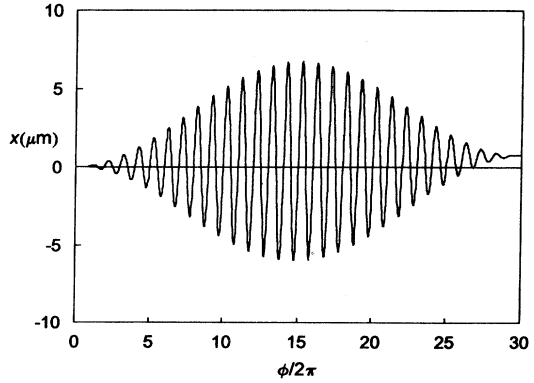

FIG. 9. Transverse electron trajectory as a function of phase, from 2D simulations. The laser parameters are $\alpha=2$, $\lambda=1$ μm, $\Delta\tau=50$ fs, and $w_0=1$ mm. The electron is injected at focus with a normalized energy $\gamma_0=10$.

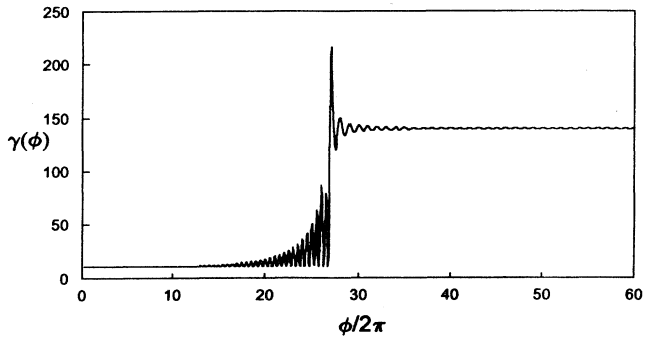

FIG. 10. Two-dimensional evolution of the electron normalized energy as a function of phase for $\alpha=3.41$, $\lambda=1$ μm, $\Delta\tau=100$ fs, $w_0=20$ μm. The electron is injected at $z=-7.6$ mm with a normalized energy $\gamma_0=10$.

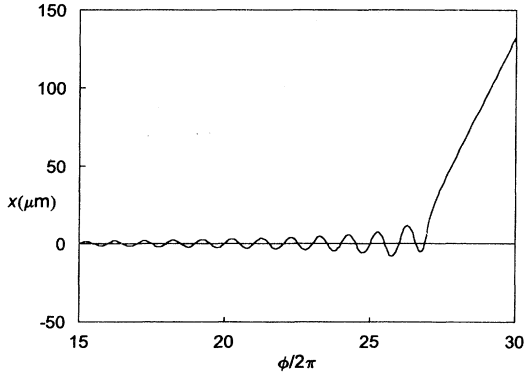

FIG. 12. Two-dimensional evolution of the electron transverse position as a function of phase, in the vicinity of focus. The parameters are the same as in Fig. 10.

In the two-dimensional analysis presented here, we consider a relativistic electron traveling along the propagation axis of the wave. We first consider the dynamics of an electron injected with $\gamma_0=10$ in the electromagnetic field of a 100 TW peak power, 1 μm wavelength, and 0.1 ps duration laser pulse, which is focused down to $w_0=20$ μm. The evolution of the electron energy as a function of its phase in the laser wave is shown in Fig. 10. The electron is overtaken by the laser pulse close to the focus ($z=-7.6$ mm), and its energy is modulated as it experiences the various phases of the electromagnetic field. In the focusing region, the laser field amplitude increases rapidly because of both spatial (focusing) and temporal (slippage towards the center of the pulse) effects. This is shown in Fig. 11, where both the spatial and temporal pulse envelopes are shown along the electron trajectory, as a function of position with respect to focus ($z=0$). As a result, the quiver amplitude increases exponentially, as shown in Fig. 12, but the particle is still confined around the propagation axis because the restoring force increases with the driving force. In close proximity to the focus, however, this situation becomes unstable as the quiver amplitude is of the order of, or exceeds, the focal spot radius. In this case, as the electron quivers through the spatial gradient of the Gaussian laser field, the restoring force decays exponentially, and the particle is scattered away from the focus, with a high energy. This is shown in Fig. 13, where the trajectory of the electron is plotted in the x-z plane, and in Fig. 14, where the field acting on the electron along its trajectory through the laser focus is presented. The scattering effect is much stronger for electrons that are seeded into the laser wave prior to focus because these electrons are confined in the laser beam until they reach focus, where they experience the strongest possible electromagnetic fields. The maximum scattering energy is obtained for those electrons which have the optimum phase $\phi=\Delta\phi$ when they are localized at the laser focus.

We now consider the dynamics of electrons injected with $\gamma_0=10$ in the electromagnetic field of a 15-TW peak power, 1-μm wavelength, 0.8-ps duration laser pulse which is focused down to $w_0=4.95$ μm. These parameters correspond to an existing Nd:glass laser system built and operating at the Lawrence Livermore National Laboratory [4,24], and yield a normalized field value $\alpha=5.34$. To show the influence of the initial position (at $\phi=0$) of the particles with respect to focus, we have calculated the escape energy of the electrons, after HPW scattering, as a function of their injection z. The results are shown in Fig. 15, which represents the axial energy spectrum of

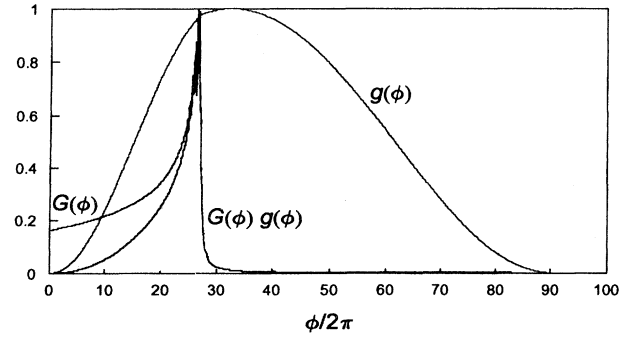

FIG. 11. Spatial and temporal laser pulse envelopes as functions of phase. The parameters are the same as in Fig. 10.

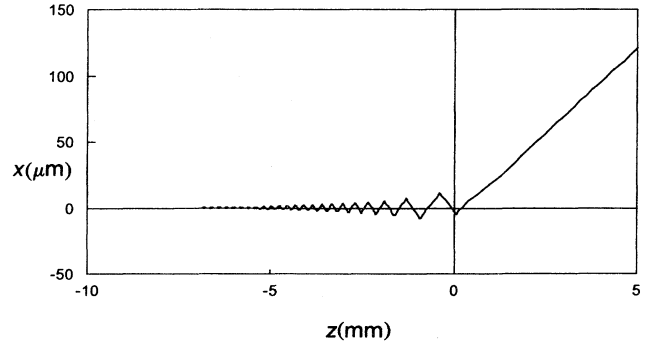

FIG. 13. Two-dimensional electron trajectory in the x-z plane. The parameters are the same as in Fig. 10.

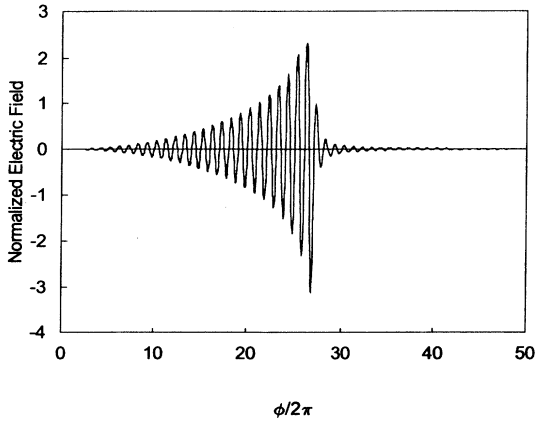

FIG. 14. Normalized electric field of the laser pulse calculated along the electron trajectory through focus, as a function of phase. The parameters are the same as in Fig. 10.

HPW scattering. The acceleration process is phase sensitive, but there is a well-defined lobe that has a fairly wide acceptance of approximately 10 mm. The peak energy is $\gamma=235$, which is within 20% of the value defined in Eq. (45), $\gamma^*=293$, in the one-dimensional theory. The transverse acceptance, which is related to the scattering cross section, is shown in Fig. 16, for the optimum injection $z=-44$ mm. The asymmetry is related to the fact that there is no particular phase relation between the laser pulse and its temporal envelope. The accelerating gradient corresponding to the parameters discussed above is 2.6 GeV/m.

As seen in the simulations presented above (see Fig. 17), there is a simple correlation between the scattering angle and the escape energy of the electron. This correlation can be expressed analytically by using the invariance of the canonical momentum in the photon field. From the expression of the two-dimensional laser field given in Eqs. (52) and (53), it is easily seen that Eq. (38) still holds, which yields

$$\gamma\beta_z=\gamma-\gamma_0(1-\beta_0)\ . \tag{76}$$

Using energy conservation, we can also write

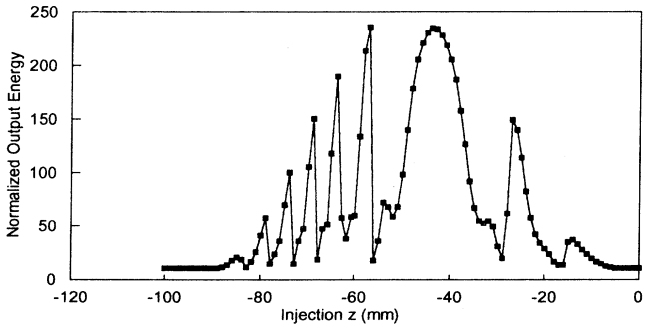

FIG. 15. Axial energy spectrum of HPW scattering. The ND:glass laser parameters are $P=15$ TW, $\lambda=1$ μm, $\Delta\tau=0.8$ ps, and $w_0=4.95$ μm. The electron is injected on-axis with a normalized energy $\gamma_0=10$.

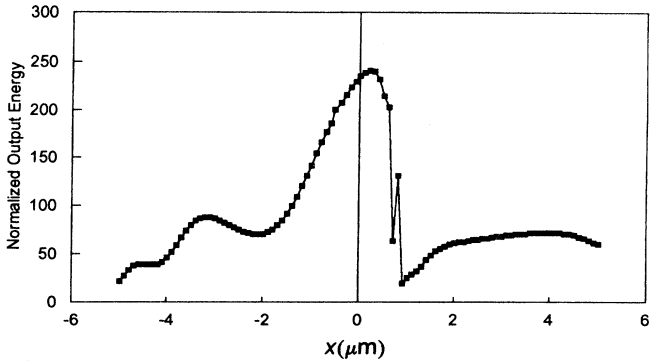

FIG. 16. Transverse acceptance of HPW scattering. The ND:glass laser parameters are $P=15$ TW, $\lambda=1$ μm, $\Delta\tau=0.8$ ps, and $w_0=4.95$ μm. The electron is injected at $z=-44$ mm with a normalized energy $\gamma_0=10$.

$$\left[\frac{\beta x}{\beta z}\right]^2=\frac{\gamma^2-1}{(\gamma\beta_z)^2}-1\ . \tag{77}$$

Combining Eqs. (76) and (77) yields the sought-after expression of the scattering angle as a function of the energy

$$\theta(\gamma)=\arctan\left[\frac{\left[\left[\left[\frac{2}{1+\beta_0}\right]\left[\frac{\gamma}{\gamma_0}-1\right]\right]\right]^{1/2}}{\gamma-\gamma_0(1-\beta_0)}\right]\ . \tag{78}$$

This theoretical function for the scattering angle is shown in Fig. 17, and the agreement between the simulated value and Eq. (78) is seen to be excellent. Therefore, this angular distribution can be considered as the signature of HPW scattering. At this point, we note that even for a fixed target experiment, such as the one described in Ref. [20], the electrons have a small initial energy. In terms of the scattering angle, this translates into a maximum scattering angle

$$\theta_{\max}=\arctan\left[\frac{1}{\gamma_0}\left[\frac{1}{2\beta_0(1+\beta_0)}\right]^{1/2}\right]\ , \tag{79}$$

which tends to 90° as the initial electron energy tends to

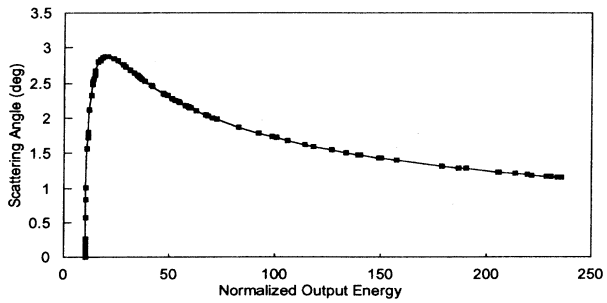

FIG. 17. Scattering angle as a function of the normalized escape energy. The squares represent 2D simulations results, while the solid line corresponds to Eq. (77). The laser parameters are the same as in Fig. 15, and $\gamma_0=10$.

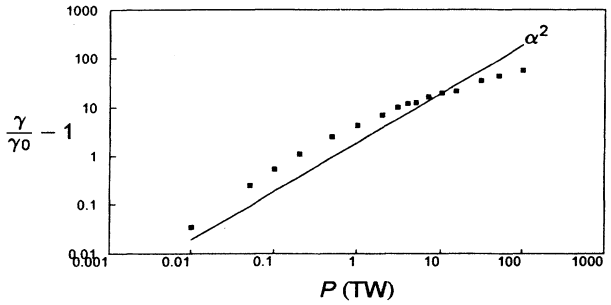

FIG. 18. Energy multiplication factor as a function of the laser power. The other laser parameters are the same as in Fig. 15, and $\gamma_0=10$.

zero. This scattering angle corresponds to electrons having acquired the energy

$$\gamma(\theta_{\max})=\gamma_0(1+\beta_0) . \tag{80}$$

This effect should be detectable at low energy, and might be a useful diagnostic of the initial energy distribution of the scattering target (for example, a pure electron plasma [25]), as $\theta_{\max}$ is a strong function of γ_0 [see Eq. (79)].

Finally, the laser intensity can be varied to study the variation of the scattering energy with the normalized field α. The results are shown in Fig. 18 and clearly show the scaling of this scattering process with the laser intensity. In this case, we have calculated the maximum energy of the scattered electrons for different values of the laser intensity, for a shorter laser pulse (50 fs FWHM), to limit the computing time. The other laser and electron parameters are 1 μm wavelength, 4.95 μm focal waist, and $\gamma_0=10$.

V. CONCLUSIONS

We have described the theoretical study of the interaction of an extremely intense, pulsed laser field (normalized field of order unity) with a single electron, in vacuum, in the vicinity of the focus. In this electrodynamic system, two very different regimes are found. At low laser intensity, the transverse quiver amplitude of the electron is small, and the effects of the transverse spatial gradients in the vicinity of focus are essentially negligible. In this case, there is no net kinetic-energy gain for the electrons, as discussed extensively in the literature. In the high power limit, or nonlinear regime, the situation is fundamentally different: the quiver amplitude imparted by the laser wave to the electron becomes comparable to the beam waist at focus, and the electron can be scattered away with a high escape energy, as the laser-electron interaction is effectively terminated within a wavelength. This effect is identified as nonlinear ponderomotive scattering, or HPW scattering. Detailed computer simulations, taking into account the transverse excursion of the accelerated electron, the temporal structure of the ultrashort laser pulse, and the effects of diffraction were presented. In the two-dimensional analysis, we consider a relativistic electron traveling along the propagation axis of the wave. The electron is overtaken by the laser pulse close to the focus, and its energy is modulated as it experiences the various phases of the electromagnetic field. In the focusing region, the laser field amplitude increases rapidly because of both spatial (focusing) and temporal (slippage towards the center of the pulse) effects. As a result, the quiver amplitude increases exponentially, but the particle is still confined around the propagation axis because the restoring force increases with the driving force. In close proximity to the focus, however, this situation can become unstable if the quiver amplitude exceeds the focal spot radius. In this case, as the electron quivers through the spatial gradient of the Gaussian laser field, the restoring force decays exponentially, and the particle can be scattered away from the focus, with a high energy. This scattering mechanism is studied in detail with a two-dimensional computer code. It was found that there is a simple correlation between the scattering angle and the escape energy of the electron. This correlation was then expressed analytically, and explained by using the invariance of the electron energy and canonical momentum in the laser field. The computer simulations show that for an injected normalized energy of 10, electrons starting to interact with the wave 44 mm before focus can be scattered by the ponderomotive potential of a 15 TW, $\lambda=1$ μm, 800 fs FWHM Nd:glass laser with a focal spot size $w_0=4.95$ μm, with energies as high as 115 MeV. The corresponding accelerating gradient is 2.6 GeV/m.

ACKNOWLEDGMENTS

This work is supported in part by Rome Laboratory (ATRI) under Grant No. F30602-94-2-0001, in part by ARO under Grant No. DAAH04-93-0084, and in part by LLNL/LDRD Contract No. W-7405-ENG-48. It is a pleasure to acknowledge useful discussions with T. E. Cowan, G. J. Caporaso, G. A. Westenskow, and J. P. Heritage.

[1] L. F. Mollenauer, R. H. Stolen, and J. P. Gordon, Phys. Rev. Lett. **45**, 1095 (1980).

[2] H. A. Haus, J. G. Fujimoto, and E. P. Ippen, IEEE J. Quantum Electron. **QE28**, 2086 (1992).

[3] P. Maine, D. Strickland, P. Bado, H. Pessot, and G. Mourou, IEEE J. Quantum Electron. **QE24**, 398 (1988).

[4] F. G. Patterson and M. D. Perry, J. Opt. Soc. Am B **8**, 2384 (1991).

[5] C. E. Clayton, K. A. Marsh, A. Dyson, M. Everett, A. Lal, W. P. Leemans, R. Williams, and C. Joshi, Phys. Rev. Lett. **70**, 36 (1993).

[6] K. Nakajima, T. Kawakubo, H. Nakanishi, A. Ogata, Y. Kato, R. Kodama, K. Mima, H. Shiraga, K. Suzuki, K. Yamakaw, T. Zhang, Y. Sakawa, T. Shoji, Y. Nishida, N. Yugami, M. Downer, D. Fisher, B. Newberger, and T. Tajima (unpublished).

[7] S. Kawata, T. Maruyama, H. Watanabe, and I. Takahashi, Phys. Rev. Lett. **66**, 2072 (1991).
[8] M. S. Hussein and M. P. Pato, Phys. Rev. Lett. **68**, 1136 (1992).
[9] M. S. Hussein, M. P. Pato, and A. K. Kerman, Phys. Rev. A **46**, 3562 (1992).
[10] E. Courant, C. Pellegrini, and Zabowicz, in *Physics and Chemistry of Protective Coatings,* edited by W. D. Sproul, J. E. Greene, and J. A. Thorton, AIP Conf. Proc. No. **149**, (AIP, New York, 1985).
[11] L. S. Brown and T. W. B. Kibble, Phys. Rev. **133**, A705 (1964).
[12] E. S. Sarachik and G. T. Schappert, Phys. Rev. D **1**, 2738 (1970).
[13] R. R. Freeman, P. H. Bucksbaum, H. Milchberg, S. Darack, D. Schumacher, and M. E. Geusic, Phys. Rev. Lett. **59**, 1092 (1987).
[14] P. B. Corkum, N. H. Burnett, and F. Brunel, Phys. Rev. Lett. **62**, 1259 (1989).
[15] P. H. Bucksbaum, L. D. Van Woerkom, R. R. Freeman, and D. W. Schumacher, Phys. Rev. A **41**, 4119 (1990).
[16] W. B. Mori and T. Katsouleas, Phys. Rev. Lett. **69**, 3495 (1992).
[17] P. L. Kapitza and P. A. M. Dirac, Proc. Cambridge Philos. Soc. **29**, 297 (1933).
[18] P. H. Bucksbaum, D. W. Schumacher, and M. Bashkansky, Phys. Rev. Lett. **61**, 1182 (1988).
[19] J. N. Bardsley, B. M. Penetrante, and M. H. Mittleman, Phys. Rev. A **40**, 3823 (1989).
[20] D. Meyerhofer, Laboratory for Laser Energetics Report No. 59, 1994 (unpublished).
[21] R. Becker, *Electromagnetic Fields and Interactions* (Blaisdell, New York, 1965), Vol. 1, Chaps. 84 and 85.
[22] I. S. Gradshteyn and I. M. Ryzhik, *Table of Integrals, Series and Products* (Academic, Orlando, FL, 1980), p. 132, Eq. 2.513.7.
[23] P. W. Milonni and J. H. Eberly, *Lasers* (Wiley Interscience, New York, 1988).
[24] F. G. Patterson, R. Gonzales, and M. D. Perry, Opt. Lett. **16**, 1107 (1991).
[25] R. Gopalan, J. Fajans, B. R. Beck, T. E. Cowan, and J. Hartley, Bull. Am. Phys. Soc. **38**, 1969 (1993).